

# Automated radiotherapy treatment planning guided by GPT-4Vision

Sheng Liu<sup>1,2\*</sup>, Oscar Pastor-Serrano<sup>1\*</sup>, Yizheng Chen<sup>1</sup>, Matthew Gopaulchan<sup>1</sup>, Weixing Liang<sup>3</sup>, Mark Buyyounouski<sup>1</sup>, Erqi Pollom<sup>1</sup>, Quynh-Thu Le<sup>1</sup>, Michael Gensheimer<sup>1</sup>, Peng Dong<sup>1</sup>, Yong Yang<sup>1</sup>, James Zou<sup>2,3†</sup>, and Lei Xing<sup>1†</sup>

<sup>1</sup>Department of Radiation Oncology, Stanford University, Stanford, CA, USA

<sup>2</sup>Department of Biomedical Data Science, Stanford University, Stanford, CA, USA

<sup>3</sup>Department of Computer Science, Stanford University, Stanford, CA, USA

## Abstract

Radiotherapy treatment planning is a time-consuming and potentially subjective process that requires the iterative adjustment of model parameters to balance multiple conflicting objectives. Recent advancements in frontier AI models offer promising avenues for addressing the challenges in planning and clinical decision-making. This study introduces GPT-RadPlan, an automated treatment planning framework that integrates radiation oncology knowledge with the reasoning capabilities of large multi-modal models, such as GPT-4Vision (GPT-4V) from OpenAI. Via in-context learning, we incorporate clinical protocols for various disease sites to enable GPT-4V to acquire treatment planning domain knowledge. The resulting GPT-RadPlan agent is integrated into our in-house inverse treatment planning system through an API. For a given patient, GPT-RadPlan acts as both plan evaluator and planner, first assessing dose distributions and dose-volume histograms (DVHs), and then providing “textual feedback” on how to improve the plan. In this manner, the agent iteratively refines the plan by adjusting planning parameters, such as weights and objective doses, based on its suggestions. The efficacy of the automated planning system is showcased across multiple prostate and head & neck cancer cases, where we compared GPT-RadPlan results to clinical plans produced by human experts. In all cases, GPT-RadPlan either outperformed or matched the clinical plans, demonstrating superior target coverage and organ-at-risk sparing. Consistently satisfying the dosimetric objectives in the clinical protocol, GPT-RadPlan represents the first multimodal large language model agent that mimics the behaviors of human planners in radiation oncology clinics, achieving promising results in automating the treatment planning process without the need for additional training.

**Keywords:** radiation therapy, treatment planning, large language models; multi-modal large language models; deep learning; artificial intelligence

## 1 Introduction

Treatment planning of modern radiation therapy (RT) modalities, such as intensity modulated RT (IMRT) and volumetric modulated arc therapy (VMAT) is an inverse process solving an optimization problem based on dose prescriptions Oelfke and Bortfeld (2001); Xing and Chen (1996); Yu and Tang (2011). This optimization problem is typically defined as a constrained optimization minimizing a weighted cost function that balances multiple conflicting objectives Webb (2003); Xing et al. (1999); Yang and Xing (2004). The result is greatly impacted by the value of the optimization parameters (e.g., the objective weights in the cost function), often resulting in plans that cannot meet all objectives at once.

A main challenge in treatment planning is translating the overall clinical goals into weighted objective functions and dose constraints yielding acceptable plans. Human planners resort to a trial-and-error approach, whereby they iteratively adjust the optimization parameters based on the results from the optimization problem until the resulting plans meet the clinical requirements Xing et al. (1999). Treatment planning is potentially subjective, since changes in the treatment parameters are based on the experience of the planner Hussein et al. (2018). Additionally, trial-and-error involves repeatedly using the computationally-expensive optimization algorithms

\*Co-first authors

†Correspondence: jamesz@stanford.edu, lei@stanford.edu

over many iterations, with potentially multiple interactions between planner and radiation oncologists in between, making the entire process time-consuming and costly, and presenting a bottleneck in precision RT.

Multiple approaches such as knowledge-based planning or multi-criteria optimization have been investigated to reduce the load on human planners Hussein et al. (2018). Knowledge-based approaches utilize prior experience to improve plans or derive good starting points for subsequent trial-and-error adjustment. Some examples include selecting closest matching patients Huang et al. (2023); McIntosh and Purdie (2016); Petrovic et al. (2016); Yang and King (2004), or using models that predict achievable dose volume histograms (DVHs) Munter and Sjölund (2015). Alternatively, the multi-criteria approach often involves a “wish list” containing objective functions with assigned priorities, which iteratively steers planning to meet as many objectives as possible ordered by their priority Breedveld et al. (2007, 2012); Voet et al. (2012, 2013).

With the recent success of deep learning, multiple neural network-based approaches have also been proposed to assist treatment planning, mostly based on U-net Ronneberger et al. (2015) or generative adversarial frameworks Goodfellow et al. (2014). Most works focus on predicting dose distributions that may be achievable based on previous clinical plans. As an input, these models take organ masks Fan et al. (2019); Ma, K. Buyyounouski, et al. (2019); Ma, Kovalchuk, et al. (2019); Nguyen et al. (2019), possibly also including beam information Barragán-Montero et al. (2019). Furthermore, these learning-based methods require large datasets and extensive training to ensure generalization across disease sites and device settings, making it difficult to integrate them into clinical workflow.

Adjusting the optimization parameters can be defined as a decision-making problem that can ideally be fully automated. Framing treatment planning as a sequence of actions taken by a planner, reinforcement learning (RL) has been recently applied to mimic human planners in RT workflows Xu et al. (2022). RL methods learn in a trial-and-error manner how to take actions maximizing a cumulative reward (i.e., a scalar based on dose metrics or target conformity). Some initial studies demonstrate that RL agents can learn to modify optimization parameters such as weights and objective doses Shen et al. (2020), while other works train agents that directly optimize machine parameters Hrinivich and Lee (2020). In practice, RL-based approaches face multiple problems. First, designing reward functions of RL that balance between different objectives — also known as the “reward design problem” - is notoriously difficult because agents are susceptible to reward hacking Norvig and Intelligence (2002); Wiering and Van Otterlo (2012). Indeed, it is not straightforward how to write a reward function to evaluate the treatment plan that requires balancing multiple clinical objectives. While RL agents can learn from labeled examples, this is not possible with a single example; RL agents need to gather large amounts of labeled data to capture the nuances of different users’ preferences and objectives, which has shown to be costly Zhang et al. (2016). Additionally, both approaches do not generalize well to new users or new environments that have different objectives, necessitating re-design or re-collection of labeled data.

Our aim is to leverage multi-modal LLMs to create an easier way for RT professionals to communicate their preferences and to facilitate the inverse treatment planning process. In the past few years, LLMs that are trained on internet-scale data have witnessed significant advancements and shown an impressive ability to learn in-context from a few examples S. Liu et al. (2023). Our key insight is that *the scale of data that multi-modal LLMs have been trained on makes them great in-context learners S. Liu et al. (2023), also allowing them to capture meaningful commonsense priors about human behavior as well as expertise on specific domains. Given a few examples and/or a description demonstrating the radiation oncologist’s objective, an LLM should be able to provide an accurate evaluation of a new test example and provide solutions for further improvement.*

In this work, we explore how to prompt multi-modal LLMs as a proxy reward function (critic) and agent (actor) for radiotherapy treatment planning. Specifically, we propose a novel framework to fully automate planning using pre-trained multi-modal LLMs. The proposed GPT-RadPlan is capable of learning to mimic human planners without any domain-specific training, using only three clinical plans as a reference, in the form of text, DVH tables, and dose distribution images. GPT-RadPlan iteratively adjusts optimization parameters, directly assessing whether the plan meets the clinical requirements based on agreement with the clinical protocol. In this case, GPT-RadPlan acts both as an evaluator and planner, first determining which aspects of the plan can be improved on the clinical requirements, and subsequently suggesting new optimization weights to address the identified deficiencies. Through our experiments, we compare GPT-RadPlan’s results to clinically approved prostate cancer and head & neck plans. There are two advantages to prompting multi-modal LLMs for treatment planning: (1) we can leverage LLM’s in-context learning abilities and prior knowledge of treatment planning so that users only need to provide a handful of examples of desirable plans and (2) we can specify our preferences intuitively using language.

## 2 Methodology

### 2.1 Problem formulation

We opt for a two-loop optimization formulation Huang et al. (2022); King et al. (1999) consisting of (i) an inner loop inverse planning step and (ii) an outer loop step optimizing the parameters of the inner loop. As such, the inner loop performs traditional fluence map optimization, trying to recover the optimal fluence map  $x$  by minimizing a cost function composed of multiple weighted objectives for different targets and organs at risk, defined as

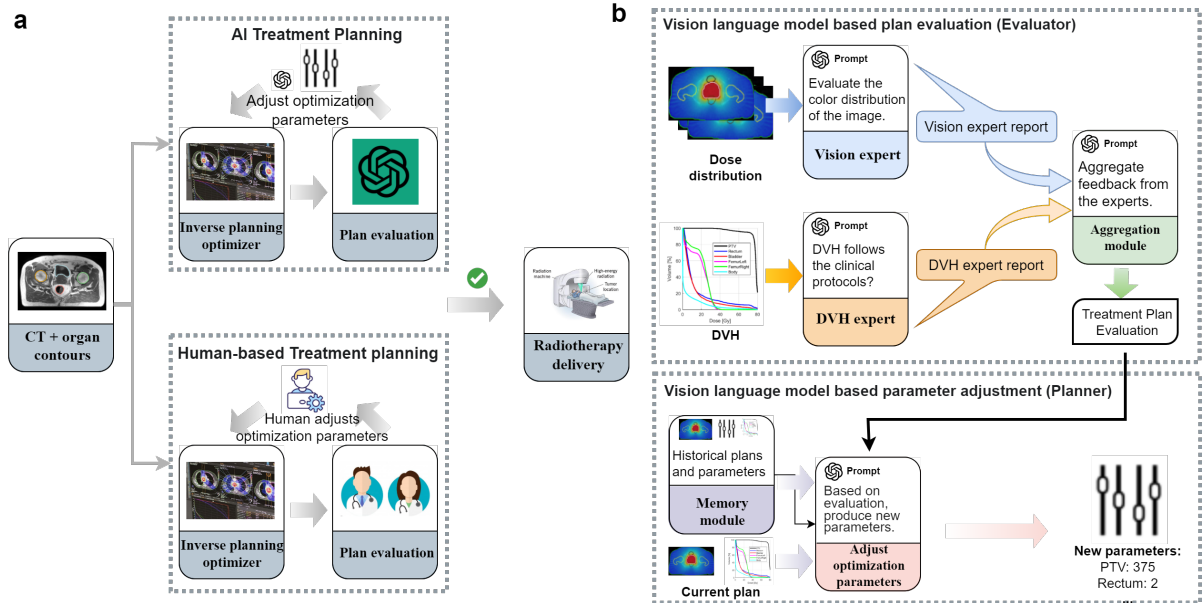


Figure 1: **Overview of GPT-RadPlan workflow.** a. Integration of multi-modal LLM-based RT treatment planning into the existing clinical workflow, using GPT-4V. GPT-RadPlan plan can communicate with the users in human language and iteratively adjusts optimization weights. b. Modules for the application of GPT-4V at different steps of the RT workflow. Based on the independent evaluation of the dose distribution by an image AI expert, and the DVH assessment from the DVH AI expert, GPT-4V reviews and/or approves the plan, providing feedback to the AI planner. The planner produces a new set of parameters based on the historical trajectory and feedback on the current plan.

$$\begin{aligned}
\min_x \quad & \sum_t w_t ([Kx]_t - d_t)^2 + \sum_s w_s \Theta([Kx]_s - d_s) ([Kx]_s - d_s), \\
\text{s.t.} \quad & D_{95}([Kx]_t) = d_t \\
& x \geq 0.
\end{aligned} \tag{1}$$

Here,  $\{w_t\}_{t=1}^{N_t}$  and  $\{w_s\}_{s=1}^{N_s}$  are the weights that balance the different objectives for  $N_t$  and  $N_s$  different PTV targets and OARs, respectively.  $K$  represents the dose influence matrix, containing the dose per unit fluence delivered to voxels in the volume by beamlets, and  $\{d_t\}_{t=1}^{N_t}$  and  $\{d_s\}_{s=1}^{N_s}$  are the scalar objective doses for each structure. Essentially, the whole cost function penalizes squared deviations from the target objective doses, regardless of the positive or negative sign, while the OAR terms only penalize squared over-dosing for doses above  $d_s$ . As such,  $\Theta$  represents the Heaviside function constraining the objective to only positive values. The minimization is constrained for only positive  $x$  values, and forcing that the  $D_{95}$  — the maximum common dose received by 95% of the structure volume — equals the prescribed dose for the targets.

We design GPT-RadPlan to operate the outer loop, finding the optimal target and OAR weights that are used to minimize Equation 1. GPT-RadPlan consists of three algorithmic components: a) environment as the context that leverages GPT-4V prior knowledge, b) vision expert that analyzes the dose distribution images, and c) DVH expert that analyzes the DVH tables and dose statistics.

## 2.2 Overall framework

As shown in Figure 1, GPT-RadPlan introduces LLM-based agents as the evaluator and planner. The system incorporates three fundamental modules to facilitate the treatment planning process, enabling iterative reasoning, planning, and continuous interaction between the agents and the treatment planning system. The task concludes either when the clinical protocols are successfully achieved or when the maximum iteration limit is reached. The functionalities of each module are as follows:

**Evaluation module** The evaluator assumes a central role within the workflow of GPT-RadPlan. It receives the present dose distribution images, DVHs, and dose statistics, enabling evaluation and learning from the planner’s historical trajectories under the context of clinical protocols. Functioning as a centralized coordinator, the evaluator engages in reasoning and providing suggestions on directions of improvement on the current plan.

Such suggestions from the critic are then used to adjust the optimization parameters and then optimize the plan, allowing for a continuous cycle of plan improvement.

To capture dose distribution images and DVHs of the treatment plan, we employ GPT-4V as a vision expert on dose distribution images and DVHs. To assist the vision expert in interpreting these images, we request GPT-4V to analyze the regional color intensity and distribution around the PTV and OARs. On the other hand, the DVH expert will take the DVH and related dose statistics as input, the DVH is first transformed into a table and then translated into a text sequence. The corresponding clinical protocol with prescribed dose and clinical requirements is also provided, so the GPT-4V can perform reasoning on the DVH based on the protocol. Aggregating the outputs of the vision expert and DVH expert, the GPT-4V provides final feedback on how to improve the current treatment plan.

For a treatment plan, we obtain its dose distribution images  $I$  and the DVH  $\delta$ , the evaluator then evaluates them to derive feedback  $f$  based on the prompt  $p$  as:

$$f = g_{\text{evaluator}}(p; I, \delta).$$

**Memory module** The memory module serves to store crucial information needed during the planning process to aid the accumulation of useful knowledge and enhance the agent’s decision-making capabilities. Specifically, the memory module is used to store the historical trajectory of the plans and the corresponding optimization parameters. The memory module also incorporates a mechanism for filtering redundant information. If the planning process is long-term, it retains only the most recent  $L$  steps of dose distribution images, DVHs, feedback and the optimization parameters  $\langle (I_{t-L+1}, \delta_{t-L+1}, f_{t-L+1}, a_{t-L+1}), \dots, (I_t, \delta_t, f_t, a_t) \rangle$ . This assists the agent in comprehending the relationship between the optimization parameters and changes in the treatment plan.

**Planning module** The planning module fulfills the vital function of converting the text-based feedback from the evaluation module to optimization parameters that can be processed by the treatment planning system. Such parameters can be beam angles for IMRT or target and OAR weights. The planning module receives the present treatment plan, and feedback from the evaluation module and extracts pertinent details from the memory module, enabling learning from its historical trajectories. Furthermore, a few examples of paired treatment plans and optimization parameters are provided to further facilitate the planning module’s understanding of the relationship between the optimization parameters and changes in the treatment plan  $a = g_{\text{planning}}(p; I_t, \delta_t, f_t)$ .

## 2.3 Dataset

This study utilizes a dataset comprising imaging and treatment plans for 11 prostate cancer patients and 6 head & neck cancer patients who underwent VMAT at the Stanford University Cancer Center. Available data for each patient includes CT scans, delineated anatomical structures, and clinically approved treatment plans obtained via Eclipse<sup>®</sup> (Varian Medical Systems, Palo Alto, CA).

For prostate cancer patients, all cases adhere to a clinical protocol designed to deliver a total dose of 70.2 Gy to the majority of the PTV. Concurrently, the protocol stipulates specific dose constraints for the OARs, which include the bladder, rectum, and both femoral heads. These dose limits typically involve upper caps on the mean OAR doses and DVH constraints, such as restricting no more than 34% of the rectum to receive in excess of 31 Gy.

Treatment plans for head and neck cancer patients follow a protocol that prescribes a dose of 70 Gy to the primary PTV. Additionally, these patients have two PTV volumes receiving doses of 56 Gy and 52 Gy, respectively. Key OARs for this group are the brainstem, spinal cord, oral cavity, larynx, and both parotid glands. The dose constraints for these OARs include upper limits on the mean dose received, with several organs also subjected to maximum dose limits.

## 2.4 Technical details and evaluation

We develop an in-house two-loop optimization system, where GPT-RadPlan performs outer loop optimization of the optimizer weights, and the inner loop fluence map optimization is based on the open-source TPS matRad Wieser et al. (2017). All plans utilize a CT and dose voxel grid with  $2.5 \times 2.5 \times 2.5 \text{mm}^3$  resolution. MatRad VMAT plans consist of co-planar arcs and are based on the SmartArc planning algorithm Christiansen et al. (2018); MacFarlane et al. (2020), using the interior-point optimization (IPOPT) package for the inverse optimization step.

Throughout our experiments, we compare the plans generated by GPT-RadPlan to their clinical counterpart, using multiple dose metrics and indexes that are frequently used in the clinic. These include the  $D_{95}$ , the homogeneity index (HI) and the conformity index (CI) and for the targets, and the  $D_5$ ,  $D_{50}$ ,  $V_{15}$  and  $V_{30}$  for the OARs.

Here, we provide a brief description of each of these metrics. First, we utilize the  $D_q$  — where  $q$  is a given percentage from 0% to 100% — to denote the common maximum dose received by  $q\%$  of the target/organ volume. Similarly, the  $V_d$  represents the percentage of the volume receiving at least a dose of  $d$  Gy. For targets, both a higher  $D_q$  close to the prescribed dose and a higher  $V_d$  close to 100% are desirable. Conversely, for OARs, both the  $D_q$  and  $V_d$  metrics would ideally be as low as possible.

Table 1: **PTV dose metrics.** Several dose metrics of the PTV target are displayed for all the clinical and GPT-RadPlan plans, including the mean and minimum doses, as well as the  $D_{95}$ , the HI and the CI. For all the metrics, we include the average values across plans and the standard deviation in brackets. Values in bold represent the best for each PTV target.

Target	Method	Mean dose [Gy]	Min dose [Gy]	$D_{95}$ [Gy]	HI	CI
Prostate plans						
PTV70.2	Goal	70.20	$\approx 70.20$	70.20	0	1.00
	Clinical	72.35 (0.63)	61.16 (2.39)	70.05 (0.15)	5.43 (1.04)	0.883 (0.021)
	GPT-RadPlan	<b>70.69</b> (0.09)	<b>63.69</b> (2.33)	<b>70.21</b> (0.01)	<b>1.96</b> (0.26)	<b>0.921</b> (0.025)
Head & neck plans						
PTV70	Goal	72.00	$\approx 70.00$	70.00	0	1.00
	Clinical	<b>71.97</b> (0.23)	60.75 (3.38)	69.69 (0.08)	<b>5.40</b> (0.51)	0.847 (0.018)
	GPT-RadPlan	72.70 (0.26)	<b>67.78</b> (1.06)	<b>70.01</b> (0.01)	6.88 (0.76)	<b>0.963</b> (0.004)
PTV56	Clinical	62.05 (1.32)	43.50 (8.41)	54.82 (2.96)	26.53 (6.91)	-
	GPT-RadPlan	<b>59.34</b> (0.56)	<b>49.46</b> (2.32)	<b>56.07</b> (0.24)	<b>14.92</b> (1.21)	-
PTV52	Clinical	54.11 (0.22)	44.49 (2.24)	52.23 (0.55)	6.83 (1.01)	-
	GPT-RadPlan	<b>53.92</b> (0.03)	<b>46.43</b> (2.40)	52.74 (0.33)	<b>3.91</b> (0.97)	-

Specifically for the target, the HI indicates whether the PTV is uniformly covered with a dose close to the prescribed value. In this study, we calculate the HI based on the  $D_5$  and  $D_{95}$  values as

$$HI = \frac{D_5 - D_{95}}{d_t} \times 100, \quad (2)$$

where lower values close to 0 indicate ideal dose homogeneity. Alternatively, the CI measures both the conformation of doses on target and the volume of surrounding tissue that is covered by the reference dose. While multiple methods have been proposed to calculate this CI, we opt for the following definition

$$CI = \frac{(TV_{95,PTV})^2}{TV \times TV_{95,Body}}, \quad (3)$$

where  $TV_{95,PTV}$  and  $TV_{95,Body}$  denotes the total volumes receiving at least 95% of the prescribed dose for the PTV and the whole body, respectively, and  $TV$  is the total body volume. In the ideal scenario, the volume receiving the prescribed dose is confined to just the PTV, and the CI tends to 1 as the numerator and denominator become equal.

Based on these metrics, we perform multiple experiments to (i) determine the optimal architecture for GPT-RadPlan’s evaluation module, and (ii) assess the quality of GPT-RadPlan’s generated plans, comparing them to the available clinical plans.

## 3 Results

### 3.1 Planning performance

To assess GPT-RadPlan capabilities in mimicking clinical human planners, we first perform a quantitative comparison between GPT-RadPlan generated plans and clinical plans based on the aforementioned metrics, including both the CI and HI, the  $D_{95}$ , mean and minimum doses for the PTV targets, and the mean dose,  $D_5$ ,  $D_{50}$ ,  $V_{15}$  and  $V_{30}$  for the OARs. We also compare the types of plans qualitatively based on the final DVH and dose distributions.

Table 1 contains the average PTV metrics across all plans for both disease sites. For the prostate cases, GPT-RadPlan’s results outperform the clinical plans across all metrics, achieving a higher minimum dose, a  $D_{95}$  that exactly matches the prescribed dose, and significantly better dose homogeneity and conformity. Similarly, GPT-RadPlan demonstrated enhanced performance over the clinical plans in the head & neck cases, showing improved metrics across all categories, albeit with a slight lag in target homogeneity for the high-dose target (PTV70). Additionally, Table 2 displays the organ-sparing metrics for the main OARs. As in the PTV case, GPT-RadPlan results in treatment plans that deliver less dose to OARs, as shown by the lower metric values across the board.

Figure 2 further confirms GPT-RadPlan’s superiority in sparing OARs. In the prostate cases depicted in Figure 3a, GPT-RadPlan achieves a sharper dose fall-off within the PTV (black line), resulting in more homogeneous delivery. Additionally, GPT-RadPlan generates plans that considerably spare the rectum compared to their clinical counterparts, while maintaining comparable doses to the femoral heads and slightly decreasing average bladder doses. In the head & neck cases illustrated in Figure 3b, the clinical plans generally result in lower doses

Table 2: **OAR dose metrics.** We show multiple dose metrics capturing OAR sparing in prostate and head & neck plans. These include the mean dose, the  $D_5$  and  $D_{50}$  (maximum common dose that 5% or 50% of the volume receives), and the  $V_{15}$  and  $V_{30}$  (representing which percentage of the volume receives 15 and 30 Gy, respectively). For all the metrics, we include the average values across plans and the standard deviation in brackets. In all cases, lower values are preferred.

Organ	Method	Mean dose [Gy]	$D_5$ [Gy]	$D_{50}$ [Gy]	$V_{15}$ [%]	$V_{30}$ [%]
Prostate plans						
Bladder	Clinical	20.42 (8.87)	63.60 (11.67)	13.18 (11.04)	42.40 (17.21)	27.56 (14.20)
	GPT-RadPlan	19.28 (7.90)	64.14 (11.04)	11.20 (8.56)	40.11 (14.84)	26.07 (12.53)
Rectum	Clinical	26.84 (6.43)	66.92 (6.91)	22.79 (6.64)	68.40 (15.46)	36.03 (10.64)
	GPT-RadPlan	22.56 (4.46)	62.57 (10.97)	16.54 (4.46)	53.91 (12.68)	26.98 (9.44)
Head & neck plans						
Brainstem	Clinical	12.25 (3.46)	31.36 (2.30)	8.60 (5.01)	32.90 (13.70)	9.74 (7.37)
	GPT-RadPlan	11.49 (4.76)	27.92 (3.24)	9.10 (6.70)	35.44 (16.31)	0.00 (0.00)
Larynx	Clinical	46.30 (12.02)	72.30 (0.60)	44.28 (16.52)	96.27 (3.44)	69.04 (20.11)
	GPT-RadPlan	40.74 (14.49)	73.16 (0.36)	35.08 (22.22)	76.48 (6.69)	55.58 (25.50)
Oral Cavity	Clinical	35.55 (1.73)	70.43 (3.31)	40.55 (18.14)	93.68 (4.46)	50.57 (3.84)
	GPT-RadPlan	31.26 (0.71)	69.89 (4.93)	24.35 (2.55)	75.60 (9.74)	38.29 (0.49)
Parotid Left	Clinical	36.36 (14.22)	61.16 (12.28)	37.35 (21.66)	74.80 (20.07)	54.53 (22.41)
	GPT-RadPlan	30.31 (15.05)	58.28 (15.80)	31.74 (22.77)	56.81 (22.79)	39.27 (25.08)
Parotid Right	Clinical	34.67 (9.31)	60.88 (10.68)	33.09 (12.09)	81.64 (19.21)	54.86 (19.70)
	GPT-RadPlan	27.42 (3.65)	60.39 (10.76)	21.64 (5.46)	61.06 (11.23)	36.74 (8.55)
Spinal Cord	Clinical	17.36 (6.74)	33.25 (5.66)	17.13 (13.53)	54.81 (12.25)	22.60 (27.89)
	GPT-RadPlan	15.67 (3.08)	30.23 (0.19)	14.26 (11.72)	54.31 (11.23)	0.00 (0.00)

to all OARs, particularly for the larynx, oral cavity, and parotid glands, which often partially overlap with the target volumes.

Due to the overlapping standard deviations noted in Table 2 and the wide shaded regions in Figure 2, GPT-RadPlan’s superiority over clinical plans in sparing OARs remains uncertain. The large standard deviations occur because the tumor targets in each patient are located in closer proximity to different OARs. For instance, two head & neck patients might each have a larger PTV overlapping either the left or right parotid gland, leading to a substantially higher dose received by the overlapping gland. We demonstrate this and prove GPT-RadPlan’s superiority in Figure 3, where the difference in dose metrics between GPT-RadPlan and clinical plans is calculated individually for each patient in the cohort. The data consistently show that GPT-RadPlan’s metrics are lower, as the boxes generally sit above the red line, confirming that GPT-RadPlan is capable of achieving plans that deliver less dose on the same patient. Overall, GPT-RadPlan plans outperforms clinical plans in 82% of the prostate patients, achieving an average 15% reduction in OAR metrics. Likewise, GPT-RadPlan provides better plans in 75% of the head & neck cases, reducing the mean dose by a 10-15% for most of the OARs.

To investigate how GPT-RadPlan acts over the multiple iterations, Figure 4 compares the dose distributions and DVHs for a prostate and head & neck patient at different iteration steps. Figure 4a depicts such “planning trajectories” for one of the prostate patients, where GPT-RadPlan first ensures homogeneous PTV coverage (uniform red color) and subsequently reduces the dose delivered to the rectum and bladder (blue and red contours, respectively). Likewise, Figure 4b demonstrates the same behavior for a head & neck patient, where GPT-RadPlan first ensures target coverage (black, purple, and magenta contours), and then progressively minimizes the dose delivered to the oral cavity and larynx (grey and green contours), as well as the overall body dose.

## 4 Discussion

The proposed GPT-RadPlan represents an advancement in the field of radiation oncology, offering a fully automated treatment planning framework that leverages the capabilities of state-of-the-art multi-modal LLMs, such as OpenAI GPT-4V. Its ability to operate without the need for domain-specific datasets or extensive training facilitates integrating GPT-RadPlan into various clinical workflows, without requiring any adjustment to current clinical software and optimization algorithms. This increased efficiency means that clinicians can deliver personalized treatment plans much faster, reducing patient wait times and allowing healthcare facilities and increasing clinical throughput. Moreover, being clinical software agnostic, GPT-RadPlan can be readily adopted across diverse treatment protocols and institutions, underscoring its broad applicability. To our knowledge, this is the first time that an automated treatment planning system based on LLMs has been proposed and demonstrated to be feasible for direct application to clinical environments without requiring any extensive model training.

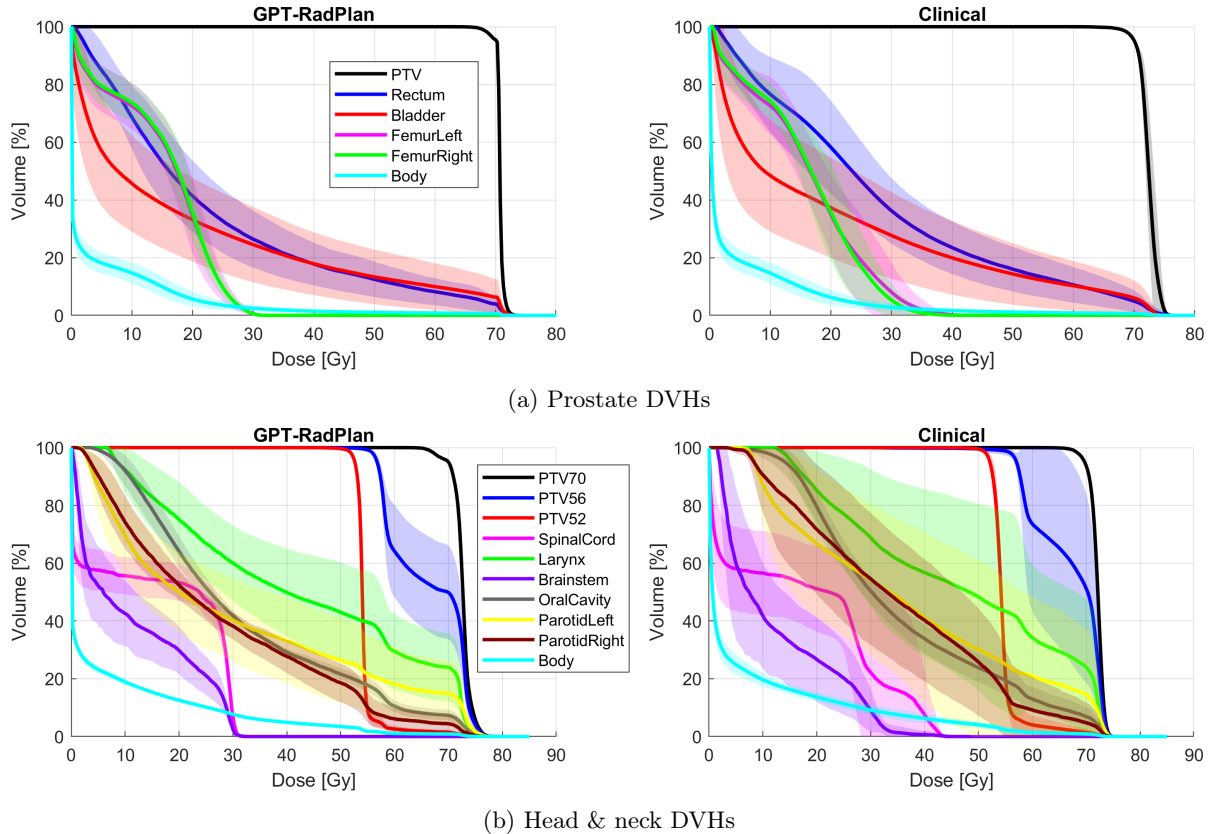


Figure 2: **DVH comparison.** Visual comparison of the DVHs for (left) GPT-RadPlan plans, and (right) clinical plans. Solid lines show the mean values, while the shaded bands indicate the standard deviation. For the OARs, better plans are usually characterized by lines that are close to the bottom left corner, implying greater OAR sparing.

GPT-RadPlan has two advantages over any other learning-based method. First, it does not require a large dataset or time-consuming training, leveraging LLM’s in-context learning abilities instead with only a handful of approved clinical plans. Moreover, users can specify clinical preferences and protocols with human language, making GPT-RadPlan a versatile tool that can generalize across disease sites, protocol requirements and metrics. As such, GPT-RadPlan can optimize plans to directly satisfy prescribed clinical criteria as defined by radiation oncologists, therefore avoiding the use of proxy metrics or crafted wish-lists. The reduced need for human interventions during planning further enhances clinical workflow and improves the allocation of human resources, freeing radiation oncologists and dosimetrists to focus on other critical aspects of patient care.

GPT-RadPlan also offers several advantages in comparison to previous RL auto-planning methods Shen et al. (2020). In general, deep RL algorithms approximate policy functions and take actions in a ‘black-box’ manner, where decisions are hardly interpretable. In contrast, GPT-RadPlan reflects on its previous results, suggesting improvements and acting based on these reflections. As a result, GPT-RadPlan actions (i.e., weight adjustments) always have an explanation. Moreover, compared to the previous RL studies requiring an entire week to train an RL agent for a specific disease site and protocol, GPT-RadPlan massively reduces computation times, being directly applicable after only minor prompt modifications. Lastly, unlike RL agents requiring a reward that hardly captures all clinical objectives and human preferences, the proposed GPT-RadPlan agents directly evaluate plans based on the entire prescribed protocol fully capturing the physician’s intent.

As demonstrated in the results, the plans generated by GPT-RadPlan uniformly cover PTV targets and spare OARs, providing a high level of consistency and quality that should contribute to better patient outcomes. After multiple iterations, GPT-RadPlan can provide plans that satisfy all the criteria in the clinical protocol for prostate cases, matching the PTV coverage requirements while always irradiating OARs with lower mean doses and DVH constraints than those indicated in the protocol. For head & neck plans, GPT-RadPlan’s plans cannot satisfy all the clinical requirements simultaneously, as is often observed in clinical practice. This involves conflicting objectives, such as sparing two different organs or prioritizing the coverage of the PTVs rather than sparing a single OAR (e.g., the larynx). Since the planner prioritizes dose objectives based on the order specified in the prompt, GPT-RadPlan could, in principle, allow for the exploration of the Pareto frontier by easily modifying these prompt priorities.

As possible next steps, instead of providing a few manually selected patients as a reference, GPT-RadPlan

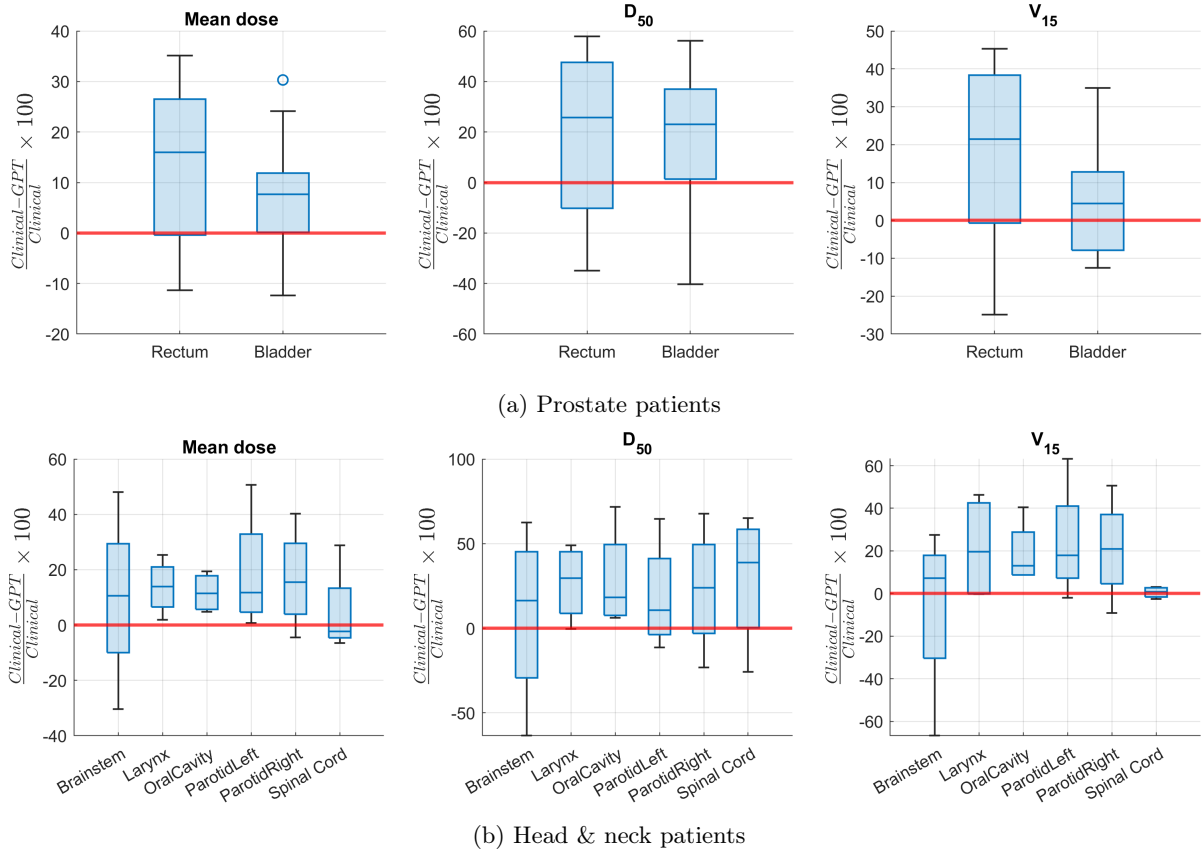


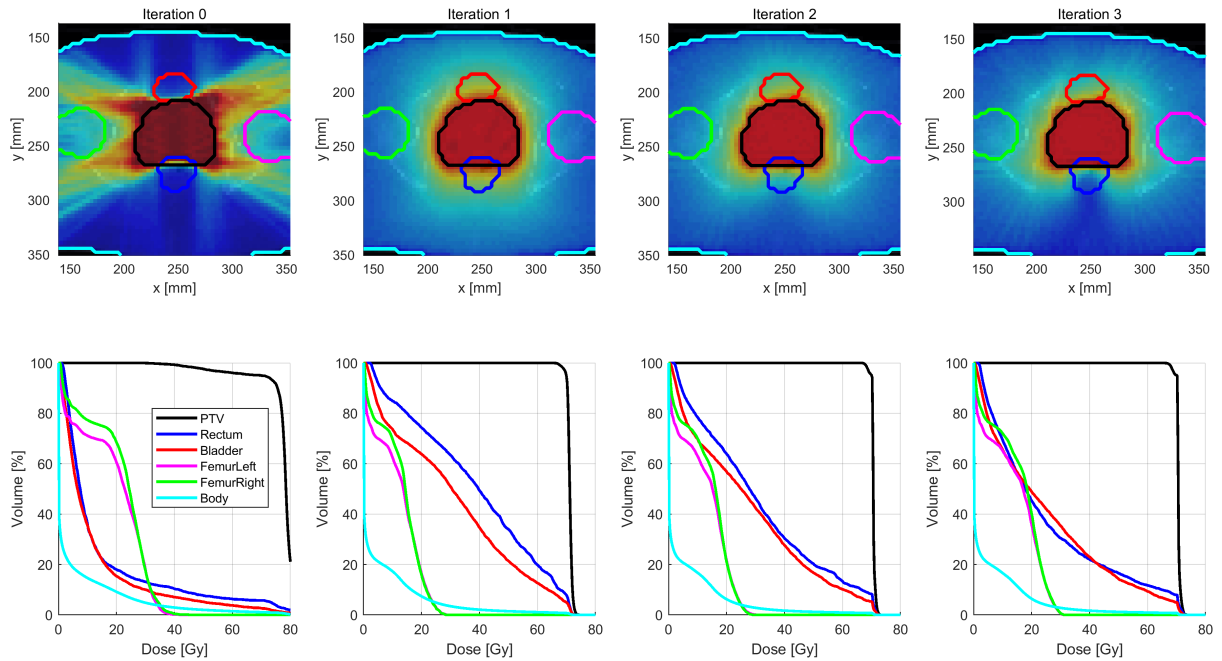
**Figure 3: Case-by-case differences between GPT-RadPlan and clinical plans.** For every relevant OAR, each box displays the relative difference between clinical and GPT-RadPlan plans of all the patients in the prostate or head & neck cohorts. Each panel shows the relative difference between different OAR metrics, including (left) the mean dose, (center) the  $D_{50}$  and (right) the  $V_{15}$ . Positive values above the red line indicate that GPT-RadPlan plans result in lower metric values, which is preferred.

could be coupled to retrieval-augmented generation (RAG) that retrieves the most similar plans in a database to be used for assistance [Huang et al. \(2023\)](#); [S. Liu, Kaku, et al. \(2022\)](#). Future work could also explore GPT-RadPlan applications to proton treatments in the presence of setup, range or anatomical uncertainties [Pastor-Serrano et al. \(2023, 2021\)](#), expanding the model capabilities to adjust robustness settings in addition to objective weights. Additionally, since one limitation of GPT-RadPlan is its lack of direct alignment with human preferences, subsequent studies could further improve model performance by manually collecting radiation oncologists’ plan evaluations and using these to fine-tune the LLMs and calibrating the LLMs [S. Liu, Kaku, et al. \(2022\)](#); [S. Liu, Zhang, et al. \(2022\)](#); [Y. Liu et al. \(2024\)](#), or using RT fine-tuned models to assist in the evaluation task [Z. Liu et al. \(2023\)](#).

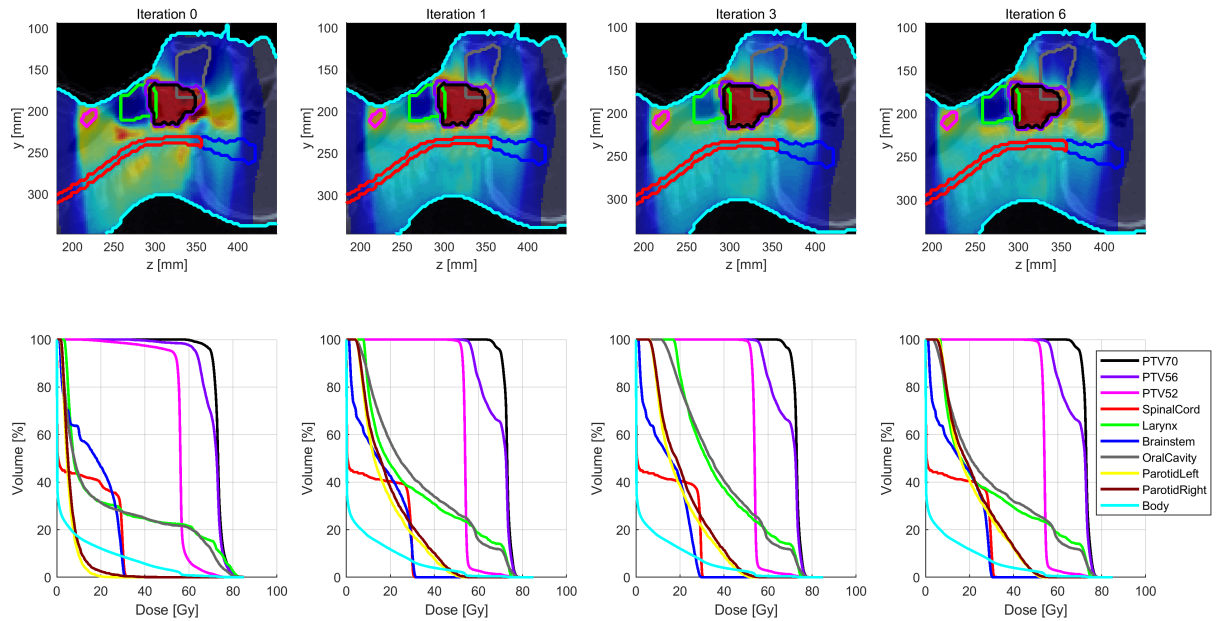
## 5 Conclusion

In this study, we present a novel GPT-RadPlan framework to enhance the collaborative performance of radiotherapy treatment planning workflow based on GPT-4V. Building upon the commonsense reasoning capabilities and domain knowledge on radiation oncology exhibited by GPT-4V, without any further fine-tuning or training on the GPT-4V, we effectively augment the planning and coordination abilities among multi-modal LLM agents through context-aware reasoning mechanisms and comprehensive feedback mechanisms, facilitating continuous interaction between the modules like planner and evaluator. GPT-RadPlan demonstrates remarkable performance in prostate and head & neck planning. Notably, it exhibits exceptional capabilities in learning from historical trajectories and mistakes in the past. We believe that with further enhancements in multi-modal LLMs, using these for treatment planning will provide new opportunities for further advancement.





(a) Prostate case



(b) Head & neck case

Figure 4: **Planning trajectories.** From left to right, each column shows the evolution of the dose distribution (2D slice centered at the iso-center) and the corresponding DVH. The top figure (a) shows one of the prostate cases requiring only 3 steps to obtain a treatment plan that meets the clinical protocol requirements, while (b) depicts the trajectory for a head & neck case requiring 6 optimization steps. As the iteration number increases, GPT-RadPlan first ensures homogeneous PTV coverage, subsequently reducing the dose delivered to the OARs.

## 6 Acknowledgement

This research was supported in part by the National Institutes of Health (NIH) grant 1R01CA256890 and 1R01CA275772.

## 7 Conflict of interest

O. Pastor-Serrano, S. Liu, J. Zou and L. Xing are co-inventors on a patent application based on this work.

## References

- Barragán-Montero, A. M., Nguyen, D., Lu, W., Lin, M.-H., Norouzi-Kandalan, R., Geets, X., . . . Jiang, S. (2019). Three-dimensional dose prediction for lung IMRT patients with deep neural networks: Robust learning from heterogeneous beam configurations. *Medical Physics*, *46*(8), 3679–3691. DOI: 10.1002/mp.13597
- Breedveld, S., Storchi, P. R. M., Keijzer, M., Heemink, A. W., & Heijmen, B. J. M. (2007). A novel approach to multi-criteria inverse planning for IMRT. *Physics in Medicine & Biology*, *52*(20), 6339. DOI: 10.1088/0031-9155/52/20/016
- Breedveld, S., Storchi, P. R. M., Voet, P. W. J., & Heijmen, B. J. M. (2012). iCycle: Integrated, multicriterial beam angle, and profile optimization for generation of coplanar and noncoplanar IMRT plans. *Medical Physics*, *39*(2), 951–963. DOI: 10.1118/1.3676689
- Christiansen, E., Heath, E., & Xu, T. (2018). Continuous aperture dose calculation and optimization for volumetric modulated arc therapy. *Physics in Medicine & Biology*, *63*(21), 21NT01. DOI: 10.1088/1361-6560/aae65e
- Fan, J., Wang, J., Chen, Z., Hu, C., Zhang, Z., & Hu, W. (2019). Automatic treatment planning based on three-dimensional dose distribution predicted from deep learning technique. *Medical Physics*, *46*(1), 370–381. DOI: 10.1002/mp.13271
- Goodfellow, I., Pouget-Abadie, J., Mirza, M., Xu, B., Warde-Farley, D., Ozair, S., . . . Bengio, Y. (2014). Generative Adversarial Nets. In *Advances in Neural Information Processing Systems* (Vol. 27). Curran Associates, Inc.
- Hrinivich, W. T., & Lee, J. (2020). Artificial intelligence-based radiotherapy machine parameter optimization using reinforcement learning. *Medical Physics*, *47*(12), 6140–6150. DOI: 10.1002/mp.14544
- Huang, C., Nomura, Y., Yang, Y., & Xing, L. (2022). Meta-optimization for fully automated radiation therapy treatment planning. *Physics in Medicine & Biology*, *67*(5), 055011. DOI: 10.1088/1361-6560/ac5672
- Huang, C., Vasudevan, V., Pastor-Serrano, O., Islam, M. T., Nomura, Y., Dubrowski, P., . . . Xing, L. (2023). Learning image representations for content-based image retrieval of radiotherapy treatment plans. *Physics in Medicine & Biology*, *68*(9), 095025. DOI: 10.1088/1361-6560/acddb0
- Hussein, M., Heijmen, B. J. M., Verellen, D., & Nisbet, A. (2018). Automation in intensity modulated radiotherapy treatment planning—a review of recent innovations. *British Journal of Radiology*, *91*(1092), 20180270. DOI: 10.1259/bjr.20180270
- Liu, S., Kaku, A., Zhu, W., Leibovich, M., Mohan, S., Yu, B., . . . others (2022). Deep probability estimation. *Proceedings of Machine Learning Research*, *162*.
- Liu, S., Xing, L., & Zou, J. (2023). In-context vectors: Making in context learning more effective and controllable through latent space steering. *arXiv preprint arXiv:2311.06668*.
- Liu, S., Zhang, X., Sekhar, N., Wu, Y., Singhal, P., & Fernandez-Granda, C. (2022). Avoiding spurious correlations via logit correction. In *The eleventh international conference on learning representations*.
- Liu, Y., Yang, T., Huang, S., Zhang, Z., Huang, H., Wei, F., . . . Zhang, Q. (2024). Calibrating llm-based evaluator. In *Proceedings of the 2024 joint international conference on computational linguistics, language resources and evaluation (lrec-coling 2024)* (pp. 2638–2656).
- Liu, Z., Wang, P., Li, Y., Holmes, J., Shu, P., Zhang, L., . . . Liu, W. (2023). *RadOnc-GPT: A Large Language Model for Radiation Oncology* (No. arXiv:2309.10160). arXiv.
- Ma, M., K. Buyyounouski, M., Vasudevan, V., Xing, L., & Yang, Y. (2019). Dose distribution prediction in isodose feature-preserving voxelization domain using deep convolutional neural network. *Medical Physics*, *46*(7), 2978–2987. DOI: 10.1002/mp.13618

- Ma, M., Kovalchuk, N., Buyyounouski, M. K., Xing, L., & Yang, Y. (2019). Incorporating dosimetric features into the prediction of 3D VMAT dose distributions using deep convolutional neural network. *Physics in Medicine & Biology*, *64*(12), 125017. DOI: 10.1088/1361-6560/ab2146
- MacFarlane, M., Hoover, D. A., Wong, E., Battista, J. J., & Chen, J. Z. (2020). Technical Note: A fast inverse direct aperture optimization algorithm for volumetric-modulated arc therapy. *Medical Physics*, *47*(4), 1558–1565. DOI: 10.1002/mp.14074
- McIntosh, C., & Purdie, T. G. (2016). Contextual Atlas Regression Forests: Multiple-Atlas-Based Automated Dose Prediction in Radiation Therapy. *IEEE Transactions on Medical Imaging*, *35*(4), 1000–1012. DOI: 10.1109/TMI.2015.2505188
- Munter, J. S., & Sjölund, J. (2015). Dose-volume histogram prediction using density estimation. *Physics in Medicine & Biology*, *60*(17), 6923. DOI: 10.1088/0031-9155/60/17/6923
- Nguyen, D., Long, T., Jia, X., Lu, W., Gu, X., Iqbal, Z., & Jiang, S. (2019). A feasibility study for predicting optimal radiation therapy dose distributions of prostate cancer patients from patient anatomy using deep learning. *Scientific Reports*, *9*(1), 1076. DOI: 10.1038/s41598-018-37741-x
- Norvig, P. R., & Intelligence, S. A. (2002). A modern approach. *Prentice Hall Upper Saddle River, NJ, USA: Rani, M., Nayak, R., & Vyas, OP (2015). An ontology-based adaptive personalized e-learning system, assisted by software agents on cloud storage. Knowledge-Based Systems*, *90*, 33–48.
- Oelfke, U., & Bortfeld, T. (2001). Inverse planning for photon and proton beams. *Medical Dosimetry*, *26*(2), 113–124. DOI: 10.1016/S0958-3947(01)00057-7
- Pastor-Serrano, O., Habraken, S., Hoogeman, M., Lathouwers, D., Schaart, D., Nomura, Y., ... Perkó, Z. (2023). A probabilistic deep learning model of inter-fraction anatomical variations in radiotherapy. *Physics in Medicine & Biology*, *68*(8), 085018. DOI: 10.1088/1361-6560/acc71d
- Pastor-Serrano, O., Habraken, S., Lathouwers, D., Hoogeman, M., Schaart, D., & Perkó, Z. (2021). How should we model and evaluate breathing interplay effects in IMPT? *Physics in Medicine and Biology*, *66*(23), 235003–235003. DOI: 10.1088/1361-6560/ac383f
- Petrovic, S., Khussainova, G., & Jagannathan, R. (2016). Knowledge-light adaptation approaches in case-based reasoning for radiotherapy treatment planning. *Artificial Intelligence in Medicine*, *68*, 17–28. DOI: 10.1016/j.artmed.2016.01.006
- Ronneberger, O., Fischer, P., & Brox, T. (2015). U-Net: Convolutional Networks for Biomedical Image Segmentation. In *Medical Image Computing and Computer-Assisted Intervention – MICCAI 2015* (pp. 234–241). Cham: Springer International Publishing.
- Shen, C., Nguyen, D., Chen, L., Gonzalez, Y., McBeth, R., Qin, N., ... Jia, X. (2020). Operating a treatment planning system using a deep-reinforcement learning-based virtual treatment planner for prostate cancer intensity-modulated radiation therapy treatment planning. *Medical Physics*, *47*(6), 2329–2336. DOI: 10.1002/mp.14114
- Voet, P. W. J., Breedveld, S., Dirkx, M. L. P., Levendag, P. C., & Heijmen, B. J. M. (2012). Integrated multicriterial optimization of beam angles and intensity profiles for coplanar and non-coplanar head and neck IMRT and implications for VMAT. *Medical Physics*, *39*(8), 4858–4865. DOI: 10.1118/1.4736803
- Voet, P. W. J., Dirkx, M. L. P., Breedveld, S., Franssen, D., Levendag, P. C., & Heijmen, B. J. M. (2013). Toward Fully Automated Multicriterial Plan Generation: A Prospective Clinical Study. *International Journal of Radiation Oncology\*Biophysics\*Physics*, *85*(3), 866–872. DOI: 10.1016/j.ijrobp.2012.04.015
- Webb, S. (2003). The physical basis of IMRT and inverse planning. *The British Journal of Radiology*, *76*(910), 678–689. DOI: 10.1259/bjr/65676879
- Wiering, M. A., & Van Otterlo, M. (2012). Reinforcement learning. *Adaptation, learning, and optimization*, *12*(3), 729.
- Wieser, H. P., Cisternas, E., Wahl, N., Ulrich, S., Stadler, A., Mescher, H., ... Bangert, M. (2017). Development of the open-source dose calculation and optimization toolkit matRad. *Medical Physics*, *44*(6), 2556–2568. DOI: 10.1002/mp.12251
- Xing, L., & Chen, G. T. Y. (1996). Iterative methods for inverse treatment planning. *Physics in Medicine & Biology*, *41*(10), 2107. DOI: 10.1088/0031-9155/41/10/018
- Xing, L., Li, J. G., Donaldson, S., Le, Q. T., & Boyer, A. L. (1999). Optimization of importance factors in inverse planning. *Physics in Medicine & Biology*, *44*(10), 2525. DOI: 10.1088/0031-9155/44/10/311
- Xu, L., Zhu, S., & Wen, N. (2022). Deep reinforcement learning and its applications in medical imaging and radiation therapy: A survey. *Physics in Medicine & Biology*, *67*(22), 22TR02. DOI: 10.1088/1361-6560/ac9cb3
- Yang, Y., & Xing, L. (2004). Clinical knowledge-based inverse treatment planning. *Physics in Medicine*

- ℳ Biology*, 49(22), 5101. DOI: 10.1088/0031-9155/49/22/006
- Yu, C. X., & Tang, G. (2011). Intensity-modulated arc therapy: Principles, technologies and clinical implementation. *Physics in Medicine & Biology*, 56(5), R31. DOI: 10.1088/0031-9155/56/5/R01
- Zhang, J., Wu, X., & Sheng, V. S. (2016). Learning from crowdsourced labeled data: a survey. *Artificial Intelligence Review*, 46, 543–576.